Compact Cascadable g_m-C All-Pass True Time Delay Cell with Reduced Delay Variation over Frequency

Seyed Kasra Garakoui, Eric A. M. Klumperink, *Senior member, IEEE*, Bram Nauta, *Fellow, IEEE*,

Frank E. van Vliet, *Senior member, IEEE*

The authors are with the University of Twente, CTIT Institute, IC Design Group, P.O.Box 217, 7500AE,Enschede, The Netherlands (e-mail: kasra.garakoui@teledynedalsa.com).(Tel: +31 61 4989772)

Abstract—At low GHz frequencies, analog time-delay cells realized by LC delay lines or transmission lines are unpractical in CMOS, due to their large size. As an alternative, delays can be approximated by all-pass filters exploiting transconductors and capacitors (g_m-C filters). This paper presents an easily cascadable compact g_m-C all-pass filter cell for 1-2.5 GHz. Compared to previous g_m-RC and g_m-C filter cells, it achieves at least 5x larger frequency range for the same relative delay variation, while keeping gain variation within 1dB. This paper derives design equations for the transfer function and several non-idealities. Circuit techniques to improve phase linearity **and** reduce delay variation over frequency, are also proposed. A 160nm CMOS chip with maximum delay of 550psec is demonstrated with monotonous delay steps of 13 psec (41 steps) and an RMS delay variation error of less than 10psec over more than an octave in frequency ($1 - 2.5$GHz). The delay per area is at least 50x more than for earlier chips. The all-pass cells are used to realize a four element timed array receiver IC. Measurement results of the beam pattern demonstrate the wideband operation capability of the g_m-RC time delay cell and timed array IC-architecture.

Index Terms—Time delay, True Time delay, All-pass filter, Phase shifter, CMOS, Timed array receiver, Phased Array Receiver, Beam forming, Beam squinting, Equalizer, Delay Compensation.

TIME delay circuits have broad applications in communication systems, e.g. for FIR and IIR filters [1], equalizers [2], and wide band beam forming [3], [4]. This paper deals with the latter application, where a "timed array" is targeted instead of the more commonly used phased array. In a timed array, true time delays are used instead of the narrowband phase shifter approximation. In this way beam squinting can be minimized [4], [5]. In beam forming receivers the variable delay cells compensate the relative delay of signals of the antenna channels. The transfer function of an ideal delay cell is: $H(s)=e^{-s\tau}$ (Fig. 1). Its gain is 1 and its phase is linear versus frequency. The delay (τ) at frequency f_0 is: $\tau(f_0)=-\varphi(f_0)/2\pi f_0$, ideally independent of f_0 (linear phase). Note that we consider true time delay here, not group delay, which is defined as $-\partial\varphi/\partial\omega$. Achieving constant true time delay is tougher as it not only requires constant group delay independent of frequency but also a constant ratio between $-\varphi$ and ω independent of frequency [6]. There are different IC compatible circuits to approximate a time delay, e.g. transmission lines [7], [8], LC delay lines [9], switched capacitor delay circuits [10] and g_m-RC or g_m-C all-pass filters [10]. However, at low GHz frequencies, transmission lines and LC delay lines in CMOS are unpractical due to the low quality factor of coils, loss of the transmission lines and their large sizes. Switched capacitor time-delay circuits on the other hand are not fast enough for low GHz applications. One of the few remaining options is to exploit an all-pass filter approximation of a delay, e.g. a 1st order all-pass filter:

$$H_{ap\_1}(s) = \frac{1-s(\tau/_2)}{1+s(\tau/_2)} \tag{1.}$$

The transfer function of this all-pass filter is plotted in Fig.. At low frequencies it approximates the ideal delay cell but at higher frequencies the delay is reduced and delay variations occur. This delay variation is quantified via the criterion $f_{\varphi=0}$ [6] which is the crossing point of the frequency axis and the tangent to the phase curve at operating frequency f_0 (Fig.). The delay variation in $\pm\Delta f$ around f_0 is approximately:

$$\frac{\tau(f_0 \pm \Delta f) - \tau(f_0)}{\tau(f_0)} \approx \frac{\frac{f_{\varphi=0}}{f_0}}{1 - \frac{f_{\varphi=0}}{f_0}} \cdot \frac{\pm \Delta f}{f_0} \tag{2}.$$

The 1st order all-pass transfer function can be realized both with g_m-RC filters [2], [11] (see Fig.3) and the g_m-C filter presented in this paper and in [12]. In [13] a benchmarking method has been proposed to compare delay cells based on $f_{\varphi=0}$. This method is re-used here to show that the g_m-C delay cell of [12] has better performance than other published designs. Moreover, the feasibility of a compact broadband beamforming IC with g_m-C delay cells is demonstrated. Apart from bandwidth, other important properties of the delay cell are: 1) Cascadability; 2) Compactness; 3) Wide delay tuning range; 4) High delay tuning resolution and precision; 5) Gain controllability; 6) Noise figure and 7) Linearity. In [12] it has been shown that the g_m-RC all-pass filters of [2] and [11] (shown in Fig.3) do not work adequately up to several GHz in UMC 180nm CMOS because of their high parasitic capacitors. Besides, they need DC blocking capacitors or source-follower buffer circuits to realize cascadability, which limits the bandwidth and/or results in high current consumption. It will be proven that the g_m-C topology of [12] has better performance: 1) Low delay variation over a 5x wider frequency band compared to other reported g_m-RC delay circuits, while maintain similar noise and nonlinearity performance; 2) Compactness compared to LC or transmission lines; 3) High resolution of delay and gain tuning; 4) Direct cascadability. Compared to [12], this paper adds circuit analysis and circuit optimization techniques, e.g. for phase linearization and bandwidth extension. The structure of this paper is as follows: in section II, the all-pass filter as an approximation of a delay cell is reviewed. In section III the all-pass filter of [12] is explained, while section IV discusses improvements of its characteristics. Section V assesses non-idealities of the delay cell. Section VI establishes a relation between requirements on the beam forming system requirements on the delay cell. Section VII presents the sub-circuits of the timed array IC and section VIII presents measurement results, while section IX draws conclusions.

The transfer function of the 1st order all-pass filter of (1) can be re-written as a combination of a

low-pass part with DC-gain of two and a unity-gain part [14] as:

$$H_{ap\_1}(s) = \frac{1-s(\tau/2)}{1+s(\tau/2)} = \frac{2}{1+s(\tau/2)} - 1 \tag{3}$$

It is realizable without floating capacitors and hence with good bandwidth potential, because the

low-pass part can be implemented by a capacitor to ground and the unity gain part does not re-

quire capacitors. Fig.4 shows the block level and g_m-RC implementation of this all-pass filter.

Aiming for direct cascadability, the g_m-C topology of Fig.5 [12] with equal input and output DC

voltages was proposed. Transistors M_1, M_4, M_5 and M_3 realize the low-pass signal path with a

DC-gain of 2. Transistors M_2 and M_3 realize the inverting unity gain path. Using PMOS transis-

tors in the "slow low-pass path" and faster NMOS transistor in the unity gain path, the useful

frequency range of the delay cell is maximized. Also, current re-use for NMOS and PMOS tran-

sistors reduces power consumption. The DC input voltage $V_{in,DC}$ results in equal drain currents

I_{DC} in M_1, M_2, M_3 and M_4, and $2I_{DC}$ for M5. Therefore, $V_{out,DC}=V_{in,DC}$. Modelling M_4 by its

small-signal g_{m4} and C as the total capacitance, the transfer function and its low frequency delay

can be written as:

$$H(s) = \frac{v_{out}(s)}{v_{in}(s)} = \frac{1-\frac{sC}{g_{m4}}}{1+\frac{sC}{g_{m4}}} \tag{4}$$

$$\tau_{LF} \approx 2C/g_{m4} \tag{5}$$

The low-frequency delay is made controllable by splitting C in switchable binary weighted ca-

pacitors. Fig.6 shows the bias circuit of the first delay cell of a delay line. It is the only cell with

an AC-coupling capacitor to the input RF signal, $V_{in,RF}$. As each signal path has this, no differ-

ence in gain and delay results. The DC voltage of V_{out} is equal to $V_{DC,bias}$. R_B is made more than

10 times larger than the source impedance of $V_{in,RF}$, for insignificant attenuation.

As the aim is to cascade cells, the non-idealities of a delay cell will now be analyzed with a capacitive load equal to the input capacitance of the next delay cell: $C_{gs,M1}+C_{gs,M2}$. In the analysis the effect of C_{gd} will be neglected as the voltage gain is low (unity gain all-pass behavior), while the right half-plane zero introduced by at g_m/C_{gd} is in the range of 50GHz for the transistors used. This is well beyond the targeting low-GHz operating frequency, and therefore for the sake of simplicity we neglected its effect. This assumption was validated by checking hand calculation versus simulation results.

A. *Finite output impedance and parasitic capacitances*

Considering finite output impedances of the transistors and the parasitic capacitors which affect the pole/zero frequency and DC gain, the transfer function of the filter becomes:

$$H(s) = \frac{1}{1+\frac{2}{g_{mn}}(g_{dsn}+g_{dsp})} \cdot \frac{1-\frac{1}{g_{mp}}(g_{dsn}+g_{dsp})}{1+\frac{1}{g_{mp}}(g_{dsn}+g_{dsp})} \cdot \frac{1-\frac{sC}{[g_{mp}-(g_{dsn}+g_{dsp})]}}{1+\frac{sC}{[g_{mp}-(g_{dsn}+g_{dsp})]}} \cdot \frac{1}{1+\frac{sC_L}{[g_{mn}+2(g_{dsn}+g_{dsp})]}} \tag{6}$$

Where g_{mn} and g_{dsn} are the transconductance and output conductance of M_1, M_2 and M_3 in saturation, g_{mp} and g_{dsp} those of M_4 and $2g_{mp}$ and $2g_{dsp}$ of M_5. The parasitic capacitances $C_{gs,M4}$, $C_{gs,M5}$, $C_{db,M4}$ and $C_{db,M3}$ are absorbed in C. Also C_L absorbs the parasitic capacitors $C_{gs,M3}$, $C_{db,M5}$, $C_{db,M2}$, $C_{db,M3}$ plus the input capacitance of the next delay cell ($C_{gs,M1}+C_{gs,M2}$). The transfer function (6) deviates from the ideal one (4) in two aspects: 1) the DC-gain is less than unity; and 2) an extra high frequency pole causes both an extra phase shift and a high frequency gain roll-off. If the following conditions are satisfied:

$$g_{mn} \gg 2(g_{dsn} + g_{dsp}) \tag{7a}$$

$$g_{mp} \gg 2(g_{dsn} + g_{dsp}) \tag{7b}$$

Then the transfer function can be rewritten as:

$$H(s) = \frac{1-\frac{2}{g_{mp}}(g_{dsn}+g_{dsp})}{1+\frac{2}{g_{mn}}(g_{dsn}+g_{dsp})} \cdot \frac{1-\frac{sC}{g_{mp}}}{1+\frac{sC}{g_{mp}}} \cdot \frac{1}{1+\frac{sC_L}{g_{mn}}} \tag{8}$$

Using the analysis in [13], the maximum usable pole frequency f_p is defined as the frequency where the gain roll-off with respect to DC is less than ΔH_p, resulting in:

$$f_p \leq \frac{g_{mn}}{2\pi C_L} \sqrt{\frac{1}{(1-\Delta H_p)^2} - 1} \qquad (9)$$

For frequencies larger than f_p, the roll-off is more than ΔH_p. Substituting $C_L \approx C_{gs,M1} + C_{gs,M2} + C_{gs,M3} = 3C_{gs,M1}$ and $f_{t,M1} \approx g_{mn}/2\pi C_{gs,M1}$ (unity current gain) in (9) results in:

$$f_p \leq \frac{f_{t,M1}}{3} \sqrt{\frac{1}{(1-\Delta H_p)^2} - 1} \qquad (10)$$

To estimate f_p and compare it with the delay cells reported in [2] and [11] (benchmarked in [13]), the same technology (UMC 180nm CMOS), same ΔH_p=1dB and same $f_{t,M1}$=12.4GHz for the NMOS transistors have been used. The choice ΔH_p=1dB is only for comparison to [13], and it will be reduced in section IV where several delay cells will be cascaded. Substituting the values in (10), the result is $f_p \leq 2$ GHz, which is a 4x improvement compared to other circuits in [13]. Fig.7 shows the simulation results of the delay cell. Reading f_p as the frequency where 45° phase shift occurs w.r.t. DC, we find $f_p \approx 1.7$GHz and a gain roll-off of ≈ 1.5dB at f_p which is due to the parasitic capacitor effects at the output of the cell. Also the DC gain is not 0dB due to the finite output impedances of transistors. In section IV the DC-gain will be calibrated to 0dB and the useful frequency range is increased further to 5x (up to 2.5GHz) that of other reported g_m-RC all-pass delay cells.

The operating bandwidth is limited to f_p, to keep the gain roll-off less than ΔH_p. Within the operating bandwidth, the value of the true time delay and group delay mainly depends on f_p, but may also be affected by the -3dB gain-roll-off frequency f_{-3dB} due to the parasitic pole at the output. Because f_{-3dB} ($\approx f_{t,M1}/3$) is much larger than f_p, a linear phase approximation can be made. This causes both a constant time delay shift and group delay shift equal to $1/2\pi f_{-3db}$. Eqn. 11 below shows expressions for both the total true time delay (τ) and group delay (τ_g) of the delay cell:

$$\tau \approx \frac{2 \tan^{-1} \frac{f}{f_p}}{2\pi f} + \frac{1}{2\pi f_{-3dB}} \tag{11-a}$$

$$\tau_g \approx \frac{f_p}{\pi(f^2 + f_p{}^2)} + \frac{1}{2\pi f_{-3dB}} \tag{11-b}$$

In both equations the second term is much smaller than the first term."

B. *Nonlinearity*

The nonlinear V-to-I conversions in M_1 and M_2 can be compensated by the I-to-V function of M_3, which are inverse functions. Also, the mirror M_4 and M_5 with gain 2, ideally renders an inverse function nonlinearity compensation. However, reactive harmonic distortion [15] occurs at frequencies well below the pole frequency. The I-V conversion by M_4 becomes more linear for higher frequencies, as the (linear) capacitor starts to dominate the I-V conversion instead of the square-root I-V function due to diode connected transistor M_4. As the V-I conversion of M_5 remains non-linear (quadratic for long transistors), the overall function is nonlinear. Due to the phase shifts caused by capacitor C, the non-linearity compensation between M_1, M_2 and M_3 is degraded. Therefore, the nonlinearity of the filters cell increases by increasing the frequency.

C. *Thermal Noise*

The input referred thermal noise of the delay cell can be written as:

$$\overline{v^2}_{in} = 8kT\gamma \left(\frac{g_{mn}+g_{mp}}{g_{mn}{}^2}\right)\left[\frac{3g_{mp}{}^2+(C\omega)^2}{g_{mp}{}^2+(C\omega)^2}\right] = 8kT\gamma \left(\frac{g_{mn}+g_{mp}}{g_{mn}{}^2}\right)\left[\frac{3\left(\frac{f_p}{f}\right)^2+1}{\left(\frac{f_p}{f}\right)^2+1}\right] \tag{10}$$

where γ is the noise excess factor of a MOSFET. As (12) shows, the input referred noise is frequency-dependent. In a delay line of n cascaded delay cells with unity gain, the total input referred noise power is n times the noise of each individual delay cell. Therefore, in systems with variable numbers of cascaded delay cells, the total noise figure will be delay dependent.

D. *PVT sensitivity*

Process, Voltage and Temperature (PVT) variations may affect the gain and amount of the delay of each delay cell. Due to mismatch and the finite output impedance of the transistors, the DC

gain of the delay cell is not exactly one. In cascaded cells these errors add-up. A tuning mechanism for DC gains is addressed in section IV. Moreover, just as for any g_m-C filters, there will be spread in the filter time-constant and hence delay due to PVT. Using master-slave techniques [16], these variations can be cancelled largely, e.g. by using replicas of the delay cell in an oscillator loop, and tuning its frequency equal to a well-known reference frequency.

IV.   DELAY CELL ENHANCEMENTS

We will now describe some techniques to reduce true time delay variation (make the delay more constant over the frequency band), extend bandwidth and (fine-) tune the delay and gain.

A. *Phase linearization (small delay variations)*

It is shown below that adding a resistor R between gate and drain of M_4 (Fig.8) improves the linearity of the phase transfer function in a limited frequency band. This can be considered as "inductive peaking" that is often used in wideband amplifiers for equalization of the gain [17]. Here, its purpose and optimization targets phase linearity and low $f_{\varphi=0}$, to minimize delay variation. The conductance $g_{m4,Lin}$ of the linearized-phase circuit inside the dashed rectangle in Fig.8 is:

$$g_{m4,Lin}(s) = g_{m4} \cdot \frac{\frac{sC_{gsM4}}{g_{m4}}+1}{sRC_{gsM4}+1} \tag{13}$$

Its value for very low and very high frequencies is $g_{m,LF} \approx g_{m4}$ and $g_{m,HF} \approx 1/R$ respectively. As is shown conceptually in Fig.9, the phase transfer function of the linearized delay cell ψ_{lin} shows a smaller value of $f_{\varphi=0}$ compared to two other phase transfer functions ψ_1 and ψ_2. Hence not only the variation in group delay is reduced but also the variation in true time delay (low $f_{\varphi=0}$).This happens for a certain optimum value of R. For low frequencies the phase curve is similar to that of an all-pass cell with its pole/zero at $\pm g_{m4}/2\pi C$ (curve ψ_1), while for high frequencies it follows the phase curve of a cell with pole/zero at $\pm 1/2\pi RC$ (curve ψ_2). For intermediate frequencies the phase curve is an interpolation between the two lines ψ_1 and ψ_2. A proper value of R found

through parametric simulations, results in a curve (ψ_{Lin}) with minimum amount of the delay variations in a band $\pm\Delta f$ around f_0, i.e. a minimum value of the criterion $f_{\varphi=0}$ (see eqn. (2)) [6], [5]. Note that closer proximity of $f_{\varphi=0}$ to zero corresponds to less delay variation vs. frequency. Fig.10 shows simulated phase curves with R as parameter. The process technology used is now 160nm CMOS and Table 1 lists the circuit parameters. $f_{\varphi=0}$ is evaluated at operation frequency of 1.75GHz (in the middle of the band 1-2.5GHz). $f_{\varphi=0}$ varies improves from -0.52GHz for R=0Ω to -0.06GHz for R=1.5kΩ(optimum). In terms of delay variation over 1-2.5GHz, using (2), a delay variation reduction from 9.8% for R=0, to 1.4% for R=1.5kΩ is found. The phase linearization resistor increases the noise figure of the delay cell by about 1.7dB.

B. *Bandwidth extension*

The load capacitor plus the parasitic capacitors at the output of the delay cell ($\approx C_L+C_{gs3}$) cause an unwanted pole and consequently gain roll-off plus an extra amount of delay. In a cascade of identical delay cells, the total load plus parasitic capacitance at the output node is $3C_{gs,M1}$. Therefore, the parasitic pole at output is: $f_{p,out}\approx g_{m3}/(6\pi C_{gs,M1})$. An active inductive peaking technique [18] is used for bandwidth extension by adding resistor R_{BWE} to convert the diode connected transistor M_3 to an "active inductor" (Fig.11). The impedance of the active inductor (the part inside the dotted box) is:

$$Z_{A-ind}(s) = \frac{1}{g_{m3}} \frac{sR_{BWE}.C_{gs,m3}+1}{s\frac{C_{gs,M3}}{g_{m3}}+1} \tag{14}$$

Choosing $R_{BWE}=1/g_{m3}$ results in $Z_{A-ind}=1/g_{m3}$. Therefore, the pole at the output becomes $f_{BWE}=g_{m3}/(4\pi C_{gs,M1})$ which means 50% bandwidth extension. Fig.12 shows the gain curve with R_{BWE} as a parameter. The transistor parameters are the same as in table 1. Theoretically, 50% bandwidth extension happens at R_{BWE} (=1/$g_{m,M3}$)=298 Ω, however, because of extra parasitic capacitance due to $C_{db,M2}$, $C_{db,M5}$, $C_{db,M3}$, $C_{gd,M2}$, $C_{gd,M3}$ and $C_{gd,M5}$ and also finite output impedances of M3, M2 and M5, simulation shows a 33% bandwidth extension. The DC gain drop of -

2dB is caused by the finite output impedance of the transistors. The bandwidth extension resistor (R_{BWE}) increases the noise figure of the delay cell by about 0.6dB. In the following subsections a technique is introduced to compensate the DC gain drop.

C. *Binary tuning of the delay*

Referring to equation (5), delay can be fine-tuned by varying C, which is designed as a 3 bit switchable binary weighted capacitor bank (see Fig.13). Because all capacitors of the bank are AC-grounded, referred to V_{supply}, they are easily switchable with PMOS transistors.

D. *Gain adjustment*

The practically achieved DC-gain of the filter is less than one because of the finite output impedance of the transistors (refer to equation (6)). In a delay line gain errors add up and there may be a need to calibrate the gains to unity. For this purpose, a switchable structure consisting of $M_{2,E}$ and $M_{3,E}$ and $M_{5,E}$ has been added (Fig.14). $M_{2,E}$ and $M_{5,E}$ work in parallel with M_2 and M_5 to increase their effective width by an amount equal to αW, so that the DC gain is multiplied by $1+\alpha$. Transistor $M_{3,E}$ sinks the excess DC current at the output point to keep the DC output bias voltage unchanged. $V_{DC,bias}$ is re-used from the biasing circuit (refer to Fig.6).

A set of binary weighted switchable gain tuning stages makes the tuning more precise (Fig 15). 3 bits have been used for the DC-gain tuning in a gain-range of 3dB (LSB≈0.4dB). Table 2 shows a comparison between the simulated results of this work and the simulated results of other reported g_m-RC delay cells (refer to Fig.3). The technology used in every case is UMC 180nm to compare to [13]. The V_{GS} of NMOS transistors for all circuits are the same to maintain equal $f_{t,n}$=12.4GHz for fair comparison. As the table shows, the pole frequency of this work is much higher (more than 5x) than other works. The NSNR [15] (defined as SNR/P@IM3=1%) criterion of the cells at 0.1GHz bandwidth was used to compare dynamic range. The NSNR of this work is 1 dB better than [11] and 6dB less than [2], partly due to IIP$_3$, but mainly due to the number of

noise contributing devices of the new delay cell [12]. Clearly, the most strong point of this work is its frequency range which is much better than for other circuits in the same technology.

<p style="text-align:center">V.   BEAM FORMING SYSTEM DESIGN</p>

In this section the timed array system specifications are related to the delay cell requirements. The formulas of this section are used in section VII to find the specifications of the sub-blocks in timed array antenna systems. Suppose we aim at N antenna elements, a frequency band from f_{min} to f_{max}, a maximum steering angle $\pm\theta_{max}$ w.r.t. the bore-sight and b bits of spatial steering resolution, while the required noise figure is less than NF_{max}. No grating lobes should exist and <-40dB null depth is targeted. From these specifications, system design parameters are extractable using [3] and [4], like the distance between antenna elements, maximum required delay, number of delay steps, and the noise figure of each channel.

To avoid grating lobes, the distance between antenna elements (d) must be less than half the wave length at the maximum operating frequency (f_{max}):

$$d \leq \frac{\lambda_{fmax}}{2} \tag{15}$$

The noise figure for N antennas improves with 10log(N) [dB] w.r.t. the noise figure for a single antenna channel. The maximum required delay per channel (τ_{max}) depends on: 1) the number of antenna elements (N), 2) the distance between antenna elements (d), 3) the maximum steering angle (θ_{max}). It can be expressed as [4] (c is the speed of the waves in the space):

$$\tau_{max} = (N-1)\frac{d.\sin(\theta_{max})}{c} \tag{16}$$

The minim delay steps (τ_{min}) depends on: 1) distance between antenna elements (d), 2) maximum steering angle (θ_{max}) and 3) spatial resolution in bits (b):

$$\tau_{min} = \frac{d.\cos(\theta_{max})}{C} \cdot \frac{\theta_{max}}{2^{b-1}} \tag{17}$$

The null depths are ideally equal to -∞, but gain mismatch will decrease the null depths. Timed array system simulations shows that for a 4-antenna array, and null depths less than -40dB, less than 0.06dB gain difference between the channels is required.

VI.   4 CHANNEL WIDE BAND BEAM FORMING IC

The designed delay cell is the basic building block of the time delay based timed array antenna IC. The IC has four antenna channels (Fig 16) [12]. Each channel applies adjustable delay and gain on the input signal. As shown in Fig 16, the adjustable delay is a combination of "Fine $\Delta\tau$" cells cascaded with "Coarse $\Delta\tau$" delay cells. The "Fine $\Delta\tau$" is realized by a cascade of three delay cells with small delay steps (refer to Fig.13). Each "Coarse $\Delta\tau$" is a cell with large delay steps (refer to Fig 15). In section VII it will be shown that 550ps total delay has been realized in a 5 bit delay resolution via "Fine $\Delta\tau$" and 6 cascaded "Coarse $\Delta\tau$" cells. The last "Coarse $\Delta\tau$" cell acts as a termination. An LNA/BALUN precedes the delay chain to reduce the noise figure. The output signals of the lines are added to each other to complete the beam forming function. Then the signal is down-converted to IF via a mixer and external LO. The total noise of the chip depends on the beam direction because the amount of the delay at each channel (number of cascaded coarse $\Delta\tau$ cells) changes with the beam direction. The maximum noise figure occurs when the beam directs toward the maximum steering angle θ_{max}. In this case the average delay of the channels is at maximum.

Analysis based on a Taylor series expansion shows that distortion has only minor impact on the phase of the fundamental frequency. Therefore the position of the null and its depth doesn't change much. However, strong signals may also generate higher harmonics with different phases than the fundamental signal in each antenna channel. After summation, the amplitude of the harmonics can add up and cause high frequency interference even if a signal comes from a null direction. Whether this is a problem depends on specific requirements and boundary conditions

which are outside the scope of this paper. Below, the functionality and circuit structure of the sub-blocks are explained.

A. LNA/BALUN

The LNA/BALUN has four main functions: 1) antenna impedance matching, 2) low noise amplification, 3) Single to differential conversion (BALUN) and 4) Gain tuning. The single to differential conversion makes the signals less sensitive to interference from other channels. It exploits a noise cancelling common gate (CG)-common source (CS) structure (Fig.17) [19]. The DC blocking capacitors C_{cg}, C_{cs} and C_{csg} are the only series capacitors in each channel. Due to a design error, their parasitic capacitance to the substrate is the main cause of the bandwidth limitation. $V_{out,cg}$ and $V_{out,cs}$ are DC fed to the "Fine $\Delta\tau$ " block. The AC gain in CG, CS stages of the LNA/BALUN can be trimmed by controlling bias voltages V_{b1} and V_{b2} to provide gain equalization and calibration. A 4 bit DAC is used to cover 1dB gain variation with 0.06dB as LSB step. This small range hardly degrades S_{11} (it remains less than -10dB) but provides the required gain resolution to provide <-40dB null depths.

B. Fine delay control

The "fine $\Delta\tau$" block realizes small delay steps. It consists of 3 cascaded delay adjustable cells (Fig.13), to cover one coarse delay step with extra margin for PVT, to prevent "missing bits". The gain of the fine $\Delta\tau$ blocks are the same for all antenna channels, therefore, it doesn't affect the beam pattern and consequently they do not require gain calibration.

C. Coarse delay control

The Coarse $\Delta\tau$ delay line consists of six cascaded delay cells, each with a fixed delay and an adjustable amount of gain. At each (voltage) output of a coarse delay cell there is a V to I converter (see Fig 16) which can be activated or not. This acts as a selectable tap to effectively

change the length (and the delay amount) of the delay line. The gain adjustability of the stages is to calibrate the gain of the coarse delay line to unity, independent of the number of cascaded blocks.

D. Selectable V to I converters

The selectable V to I converters fulfill two tasks: They select the desired output of the delay chain and they convert the signal from voltage to current. The input capacitance of the V to I converter has an effect on the delay of the channel but because this delay shift is equal for all channels it does not affect the beam pattern. However, they limit the bandwidth. Because the signals are converted to current, the summation function required for beam forming can be implemented by simply connecting all outputs together.

E. LO, Mixer and output buffer

An external differential LO is used to down-convert the beam formed signal to IF. The circuit and its outputs are differential and an active gilbert cell mixer is used with load resistors. The output voltage is buffered via source followers to match the output impedance to 50Ω.

VII. CHIP IMPLEMENTATION AND MEASUREMENTS

To demonstrate wideband beamforming, a 4-channel beam forming chip was designed in 160nm CMOS, covering more than one octave of bandwidth from 1GHz to 2.5 GHz. The beam can be steered from -60° to 60° related to bore-sight in 4 bits resolution. To avoid grating lobe conditions, the required inter-element antenna distance is $0.5\lambda_{2.5GHz}\approx$6cm (refer to (15)). The maximum required delay in each channel is found from (16) and is: τ_{max}=510psec. The delay step size is derived from the 4 bit beam steering resolution (refer to (17)): $\tau_{min}\approx$13psec. The τ_{max} to τ_{min} ratio shows that for 4 bit steering angle resolution 5 bit delay-resolution is needed per channel. The targeted average noise figure of the channels when the beam steers towards $\theta_{max}=\pm60°$ is 8dB at the mid of the frequency range (f_0=1.75GHz), i.e. the noise figure of each channel at

255psec delay must be 8dB. The 255psec delay consists of 3 cascaded coarse $\Delta\tau$ cells besides fine $\Delta\tau$. A single ended to differential voltage gain of 13 dB for each channel and 3.5dB noise figure for the LNA/BALUN theoretically results in 8.9 dB noise figure for every individual delay cell. Keeping overdrive voltage of transistors similar to table 1 results in 3.6mA current for each individual delay cell. In this test chip the simple bias circuit of Fig.6 consisting of a diode connected N- and PMOS was used. Reduction of the supply directly decreases the current and consequently affects the g_m, noise and time-delay of the delay cell. To stabilize performance either a voltage regulator will be needed, or a bias current source should be used to bias M6 and M7 in Fig.6. Fig 18 shows the chip photograph. For each channel, the delay vs. frequency over the whole frequency band and for all settings was measured. An effective number of bits for the delay setting equal to ENOB=4.7 (NOB=5) was found (Fig.19). The delays are approximately constant within <10psec variation in the operating frequency band of 1-2.5GHz. The flatness of the delay curves in Fig.19 is an immediate result of the applying the technique in Fig.9 and Fig.10 to linearize the phase vs. frequency and demonstrates that the optimization approach is highly effective. Substituting the maximum delay variations (10psec) and the maximum amount of delay ($\tau(f_0)$=550psec) in (2), we find $f_{\varphi=0} \approx 0.06$GHz at the mid of the frequency band (f_0=1.75GHz) which is close to the circuit simulations shown in Fig.10.

 Fig 20 shows the gain vs. frequency variations for all delay and gain settings (without the effect of the LNA/BALUN gain trimming). For all delay settings the gain varies less than ±1.8dB at each individual frequency point from 1GHz to 2.5GHz band. For each delay setting (A fixed delay) the gain vs. frequency variations from 1GHz to 2.5GHz remains less than 2.8dB (or ±1.4dB with respect to its average). The gain adjustability in the BALUN provides another opportunity to trim the gain of the individual frequency points with 0.03dB resolution. The gain variations vs. all delay amount settings with the help of BALUN gain trimming is: ±0.03dB over 1 to 2.5 GHz band (non-simultaneous). This gain equality resolution results in deep null depths

of the beam pattern which will be shown later (Fig 22). The gain, noise figure and input matching (S_{11}) vs. frequency of a single receiver channel set at 255psec delay is shown in Fig.21. The 255psec is the average delay of the 4 channels when the beam steers towards its maximum angle (θ_{max}) which results in the maximum noise figure for the timed array (worst case scenario). For other steering angles the average delay of the channels is less and therefore the noise figure is better. The measured gain and noise figure is in agreement with the simulations within 0.9dB.

The measured beam pattern was compared with a simulated ideal time delay based beam forming system as shown in Fig 22. For the frequency range from 2 to 2.5GHz, the -3dB beam width varies from 63° to 51° and the null to null distance from 37° to 29°. Also a new null appears at -38° in the pattern both in measurement and simulation.

The method used for beam pattern measurement is as follows: 4 RF signals representing the antenna signals are generated via 4 external RF generators. Experiments were done at 2GHz and 2.5 GHz, while an external 3GHz signal is applied to the LO input. The beam formed signal is down-converted to 500MHz to 1GHz. Going through all delay settings the beam patterns for 2GHz and 2.5 GHz are synthesized. Comparing to the simulated beam pattern, it can be seen (Fig 22) that spatial directions for the beam and nulls in the measured pattern closely follows the ideal pattern. The null depths of the beam pattern was limited to -24dB which is caused by the cross talk between the off-chip transmission lines of the antenna channels.

Table 3 [24] compares several reported delay circuits implemented via different technologies and topologies. Compared to other methods, the proposed circuit provides the lowest amount of delay vs. frequency variation (1.8% over more than an octave of bandwidth). Also it is the most compact delay circuit which provides between 1 and 2 orders of magnitude more delay per area. Therefore this circuit is one of the best candidates for low GHz RF band applications requiring large amounts of delay. Table 4 shows a comparison between our g_m-RC timed array chip and two other reported time delay based chips designed for beamforming, which exploit LC delay lines and transmission lines. The compactness of the delay cells allows us to implement the chip

in much smaller area at comparable power consumption conditions. The reported noise figure of this circuit is higher, but it is for the worst case scenario (maximum steering angle: $\theta=\pm60°$). Steering to smaller angles (referred to the bore-sight) requires less delay and produces less noise. The reported Amplitude vs. frequency variations (±1.4dB) is instantaneous for the 1-2.5GHz frequency band at each delay settings. The gain trimming property of the LNA plus gain calibration of the delay cells provide 0.03 dB resolution for individual frequencies.

VIII.   CONCLUSIONS

This paper presented a compact all-pass g_m-C cell that was compared to other reported g_m-RC delay cells, showing 5x higher operating frequency range. A chip implementation of the delay cell in 160nm CMOS results a flat gain up to 2.5GHz for the delay cell, with the help of an bandwidth extension technique. The delay cells are directly cascadable to realize a delay line without AC-coupling or buffering. This avoids parasitic capacitances to ground from DC blocking capacitors which limit frequency range or require extra current consumption. The circuit exploits current re-use with a slow PMOS low-pass path in parallel to a fast NMOS unity gain path to maximize the useful frequency range. Bandwidth and phase linearity is further enhanced by adding carefully dimensioned resistors to the diode-connected transistors. Gain fine control in the delay cells allows for precise gain calibration, independent of delay. Using simulation, a direct comparison of the new delay cell with existing g_m-C and g_m-RC delay cells has been made in terms of frequency range, dynamic range and power consumption. The SNR/P at 1% IM3 of the designed delay cell is 1dB better than [11] and 6dB worse than [2], while the frequency range is at least 5x larger (compared to [2] and [11]). To validate performance, a 4 antenna beamforming receiver chip with a maximum steering angle θ_{max} of $\pm60°$ was designed in 160nm CMOS technology with a total delay per channel of 550 psec in an area of 0.15 mm^2. Compared to other chips with LC delay lines and transmission lines, this is about 2 orders of magnitude more delay per area. The 550 psec delay is digitally controllable in 13psec steps. Delay varia-

tion over a bandwidth from 1 to 2.5GHz is less than 10 psec, which is only 1.8% of the realized delay. In other words, the selectable delays are monotonous, with low RMS error in the frequency band and therefore easy to use in calibration schemes. The delay/size of the circuit which is 7857 ps/mm^2 is at least 50x more than other delay circuits reported in literature which makes it quite suitable for low GHz operations that need large amounts of delays. An effective delay resolution of 4.7bits is demonstrated which corresponds to an effective spatial beam steering resolution of 3.5 bits for full scale steering range of ±60°, i.e. 10.6° spatial angle resolution. The average noise figure of each antenna channel in the worst case scenario (when the average delay in 4 channels is maximum, i.e. a beam direction is at ±60°) is 10dB.

REFERENCES

[1] A. V. Oppenheim, R. W. Schafer and J. Buck, "Filter Design Techniques," in *Discrete-Time Signal Processing*, 2nd ed., New Jersey, Pretince-Hall, 1999, ch. 7, sec. 1, pp. 440-449.

[2] J. Buckwalter and A. Hajimiri, "An active analog delay and the delay reference loop," *IEEE RFIC Symp., 2004,* pp. 17-20.

[3] H. J. Visser, "Antennas," in *Array and Phased Array Antenna Basics*, West Sussex, England, Wiley, 2006, ch. 2, sec. 5, pp. 76-80.

[4] R. J. Mailloux, "Phased Arrays in Radar and Communication Systems," in *Phased Array Antenna Handbook*, 2nd ed., Norwood, Artech house, 2005, ch.1, sec. 3, pp. 44-60.

[5] S. K. Garakoui, E. A. M. Klumperink, B. Nauta and F. E. van Vliet, "Phased-array antenna beam squinting related to frequency dependency of delay circuits," *EuRad Conf., 2011,* pp. 416-419.

[6] S. K. Garakoui, E. A. M. Klumperink, B. Nauta and F. E. van Vliet, "Time delay circuits: A quality criterion for delay variations versus frequency," *IEEE ISCAS Proc., 2010,* pp. 4281-4284.

[7] F. Ellinger, "Passive Devices and Networks," in *Radio Frequency Integrated Circuits and Technologies*, Berlin, Germany, Springer, 2007, ch. 6, sec. 1, pp. 195-198.

[8] F. E. van Vliet, M. van Wanum, A. W. Roodnat and M. Alfredson, "Fully-integrated wideband TTD core chip with serial control," *Gallium Arsenide applications symp., Munich,* pp. 89-92, 2003.

[9] T. Chu, J. Roderick and H. Hashemi, "An Integrated Ultra-Wideband Timed Array Receiver in 0.13 μm CMOS Using a Path-Sharing True Time Delay Architecture," *IEEE J.Solid-State Circuits, vol.42, no. 12,* pp. 2834- 2850, Dec. 2007.

[10] B. Razavi, Design of Analog CMOS Integrated Circuits, New York: McGraw-Hill, 2001,

ch. 12, sec. 2, pp. 410-423.

[11] P. Horowitz and w. Hill, "Unity-gainphase splitter," in *The Art of Electronics*, 2nd ed., New York, Cambridge University Press, 1999, ch. 2, sec. 8, pp. 77-78.

[12] S. K. Garakoui, E. A. M. Klumperink, B. Nauta and F. E. van Vliet, "A 1-to-2.5GHz phased-array IC based on gm-RC all-pass time-delay cells," *IEEE ISSCC Dig. Tech. Papers, 2012,* pp. 80-82.

[13] S. K. Garakoui, E. A. M. Klumperink, B. Nauta and F. E. van Vliet, "Frequency Limitations of First-Order gm - RC All-Pass Delay Circuits," *IEEE T. on Circuits and Systems II, vol. 60, no. 9,* pp. 572-576, Aug. 2013.

[14] K. Bult and H. Wallinga, "A CMOS analog continuous-time delay line with adaptive delay-time control," *IEEE J. Solid-State Circuits, vol. 23, no. 3,* pp. 759- 766, June 1988.

[15] K. Bult, "Harmonic Performance," in *Analog Cmos square-law circuits, PhD Thesis*, Enschede, University of Twente, 1988, ch. 6, sec. 4, pp. 93-98.

[16] B. Nauta, "Tuning," in *Analog Cmos Filters for Very High Frequencies*, Enschede, The Netherlands, Springer, 1992, ch. 5, sec. 2, pp. 139-141.

[17] B. Razavi, "Prospects of CMOS technology for high-speed optical communication circuits," *Solid-State Circuits, IEEE Journal of , vol.37, no.9,* pp. 1135-1145, Sep. 2002.

[18] T. H. Lee, "noise," in *The Design of CMOS Radio-Frequency Integrated Circuits*, 2nd ed., Cambridge University Press, 2003, ch. 11, pp. 361-362.

[19] S. C. Blaakmeer, E. A. M. Klumperink, D. M. W. Leenaerts and B. Nauta, "The BLIXER, a Wideband Balun-LNA-I/Q-Mixer topology," *IEEE J. Solid-state Circuits, vol. 43, no.12,* pp. 2706-2715, Dec. 2008.

[20] E. A. M. Klumperink and B. Nauta, "Systematic comparison of HF CMOS transconductors," *IEEE T. on Circuits and Systems II, vol. 50, no. 10,* pp. 728- 741, Oct.

2003.

[21] J. Roderick, H. Krishnaswamy, K. Newton and H. Hashemi, "Silicon-Based Ultra-Wideband Beam-Forming," *IEEE J. Solid-State Circuits, vol. 41, no. 8,* pp. 1726- 1739, Aug. 2006.

[22] H. Veenstra, M. Notten, D. Zhao and J. R. Long, "A 3-channel true-time delay transmitter for 60GHz radar-beamforming applications," *ESSCIRC Proc., 2011,* pp. 143-146.

[23] T. Chu and H. Hashemi, "A true time-delay-based bandpass multi-beam array at mm-waves supporting instantaneously wide bandwidths," *IEEE ISSCC Dig. Tech. Papers, 2010,* pp. 38-39.

[24] A. C. Ulusoy, B. Schleicher and H. Schumacher, "A Tunable Differential All-Pass Filter for UWB True Time Delay and Phase Shift Applications," *IEEE Microwave and Wireless Components Letters,* pp. 462- 464, 2011, vol. 21, no. 9.

[25] E. Adabi and A. M. Niknejad, "Broadband variable passive delay elements based on an inductance multiplication technique," *IEEE RFIC Symposium, 2008,* pp. 445- 448.

[26] Q. Ma, R. Mahmoudi and D. M. W. Leenaerts, "A 12ps true-time-delay phase shifter with 6.6% delay variation at 20-40GHz," *IEEE RFIC Symposium, 2013,* pp. 61-64.

Captions:
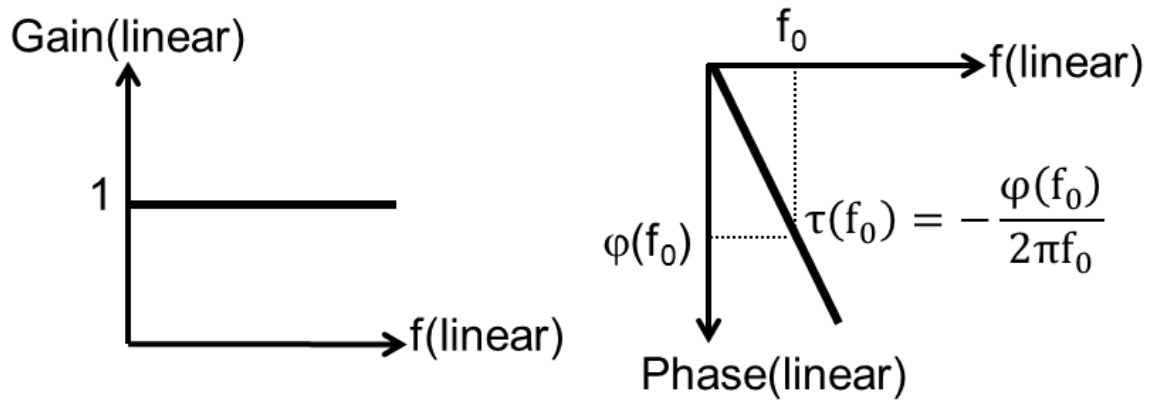
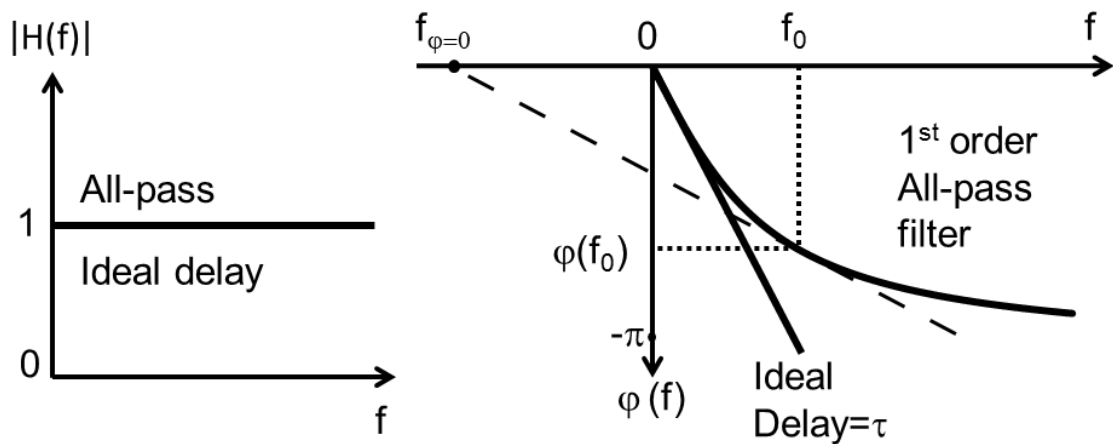Fig. 1. The gain and phase transfer function of an ideal time delay cell

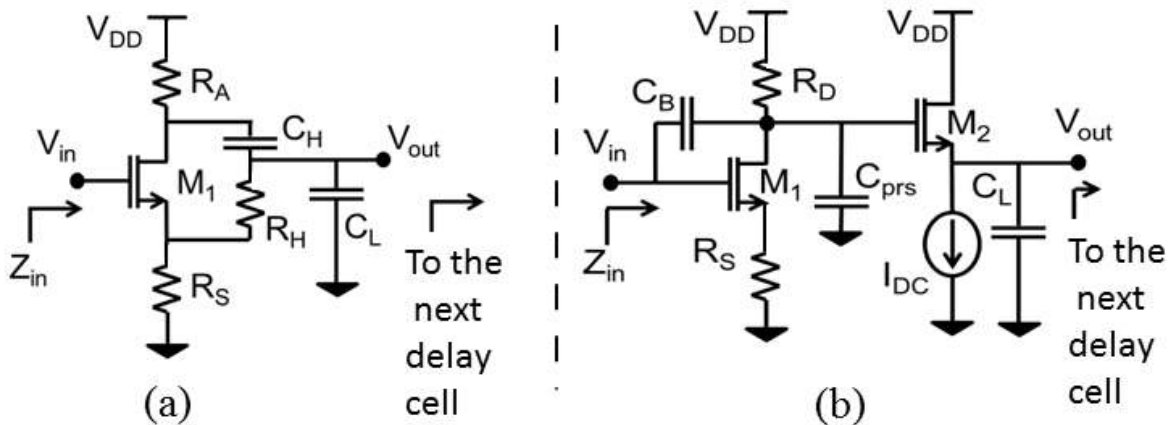Fig.2. 1st order all-pass filter with extrapolation point $f_{\varphi=0}$ vs. ideal delay (linear scales)

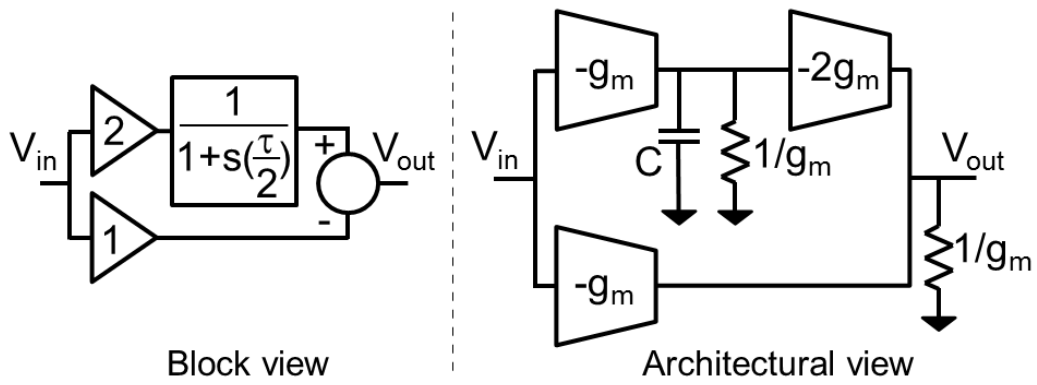Fig.3. Two known g_m-RC delay circuits: a) of [11] and b) [2]

Fig.4. The block view and architectural view of the 1st order all-pass filter implementable with no floating caps
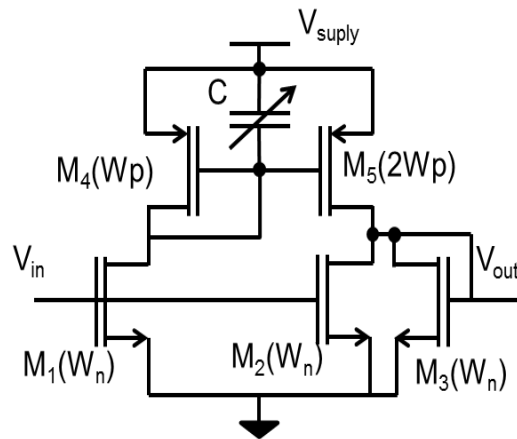
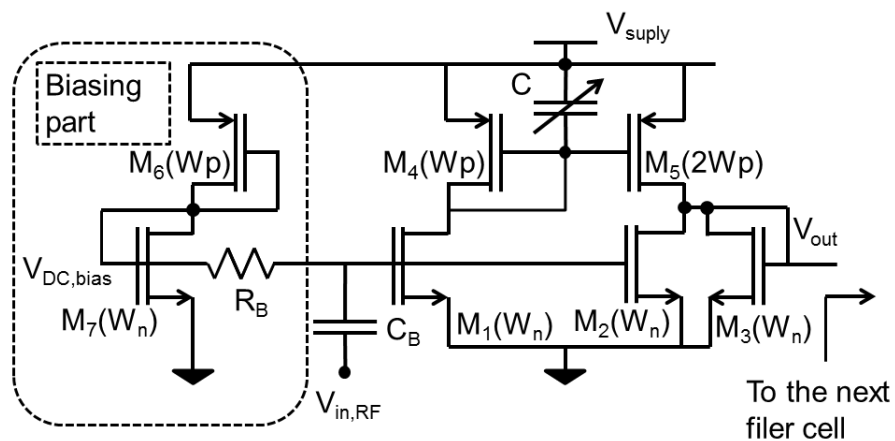Fig.5. The proposed 1st order g_m-C all-pass filter in [12].

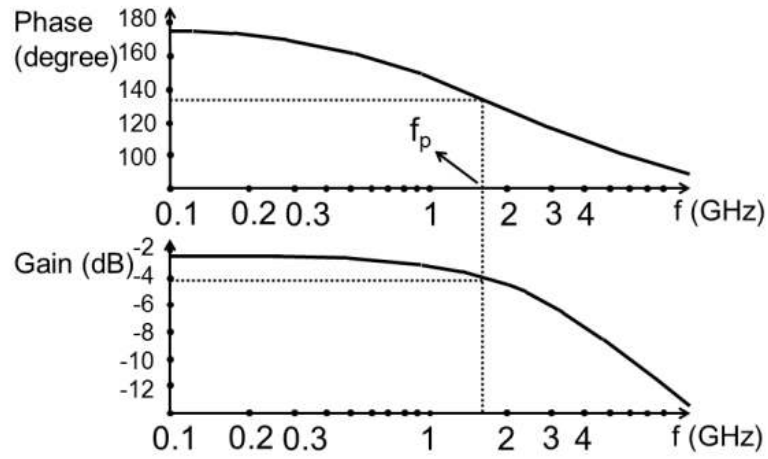Fig.6. The biasing circuitry of the first filter cell in a cascade line

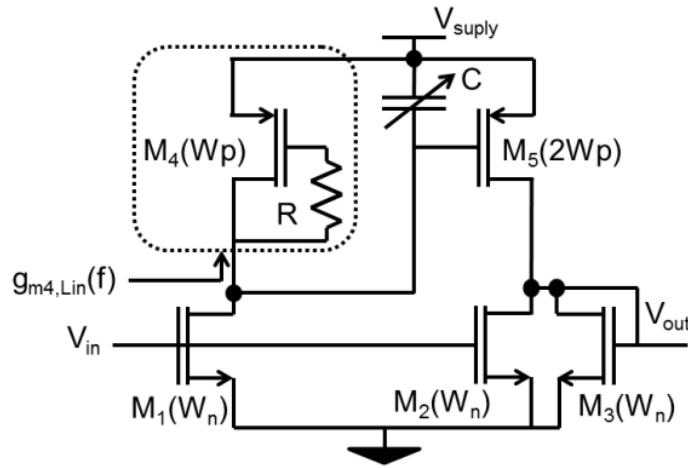Fig.7. The phase at the gate of M5, and the output of the delay cell in a delay line
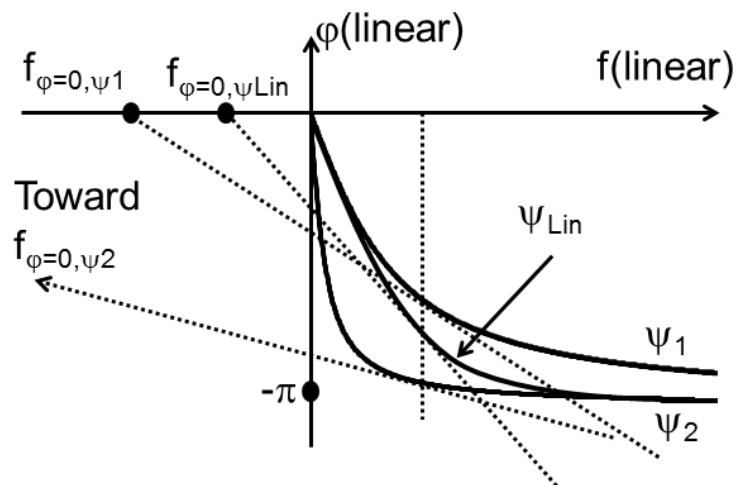
Fig.8. The phase linearization technique

Fig.9. Low frequency linearization technique of the phase transfer curve of the filter (conceptually depicted)

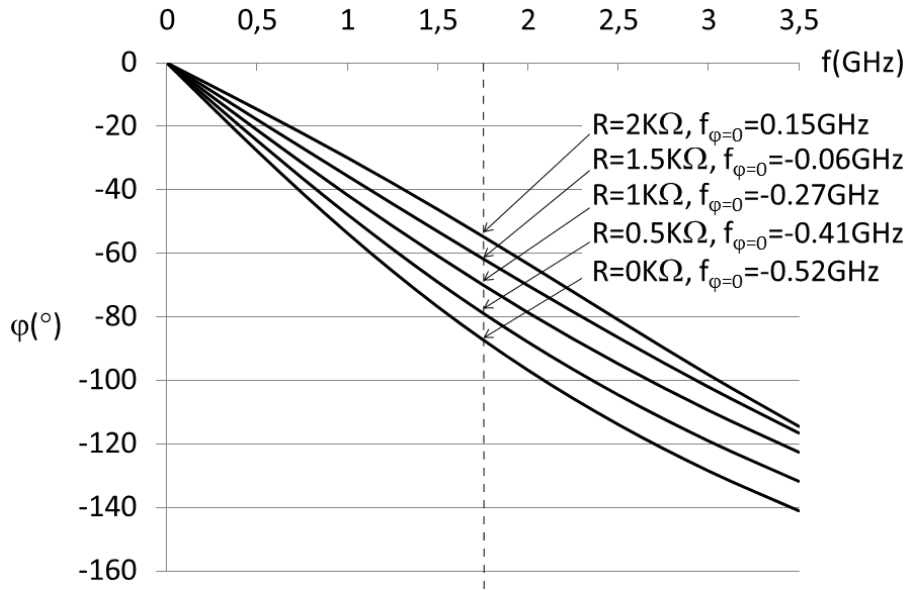Fig.10. Simulation results of the phase linearization technique for the parameters shown in table 1

Fig.11: Bandwidth extension of the filter

Fig.12. Simulation of bandwidth extension technique (R_{WBE} as a parameter)

Fig.13: The delay cell with 3 bit delay selection.

Fig.14: Adding gain tuner to the delay cell

Fig 15. Adding 3-bit gain calibration to the filter

Fig 16. The timed array IC: block level [12]

Fig.17: LNA/BALUN

Fig 18. The chip photograph

Fig.19. Delay versus frequency for all delay settings.

Fig 20. Gain of the delay line (fine tune and coarse tune) vs. f for all delay settings

Fig.21: Gain, input matching and noise figure when delay of the channel is 255ps.

Fig 22. The measure beam pattern compared to a simulated ideal beam pattern.

Table 1. The transistor parameters of the simulated delay cell

Table 2. Comparison between simulated delay cells

Table 3. benchmarking and comparison between different reported delay cells.

Table 4. Comparison between this works and two other time delay based timed array systems

Fig. 1. The gain and phase transfer function of an ideal time delay cell

Fig. 2. 1st order all-pass filter with extrapolation point $f_{\varphi=0}$ vs. ideal delay (linear scales)

Fig. 3. Two known g_m-RC delay circuits: a) of [11] and b) [2]

Fig. 4. The block view and architectural view of the 1st order all-pass filter implementable with no floating caps

Fig. 5. The proposed 1st order g_m-C all-pass filter in **[12]**

Fig. 6. The biasing circuitry of the first filter cell in a cascade line

Fig. 7. The phase at the gate of M5, and the output of the delay cell in a delay line

Fig. 8. The phase linearization technique

Fig. 9. Low frequency linearization technique of the phase transfer curve of the filter (conceptually depicted)

	W/L(μm/μm)	V_{th}(V)	I_D(μA)	V_{GS}(V)	V_{DS}(V)
M_1	13.76/0.25	0.465	488	0.714	0.714
M_2	13.76/0.25	0.465	488	0.714	0.714
M_3	13.76/0.25	0.465	488	0.714	0.714
M_4	10.64/0.25	0.449	488	1.086	1.086
M_5	21.28/0.25	0.449	976	1.086	1.086

Table 1. The transistor parameters of the simulated delay cell

Fig. 10. Simulation results of the phase linearization technique for the parameters shown in table

1
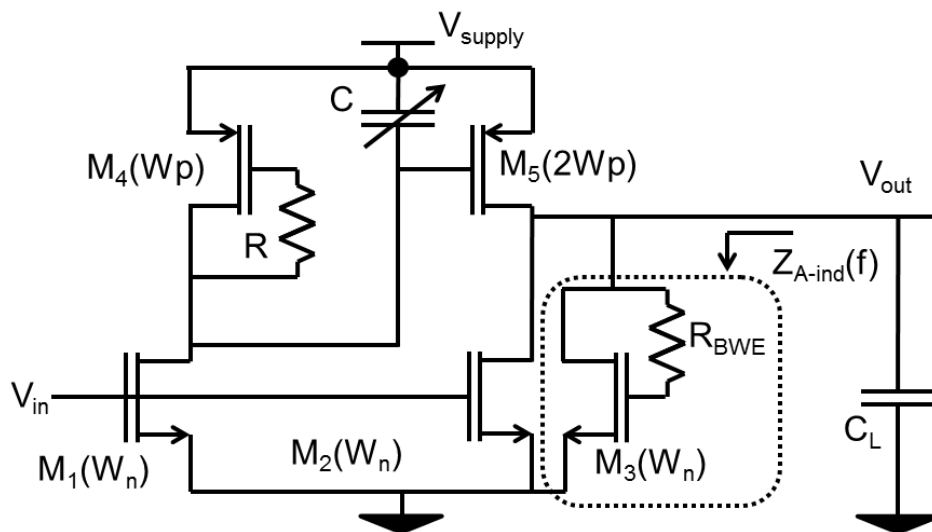
Fig. 11. Bandwidth extension of the filter
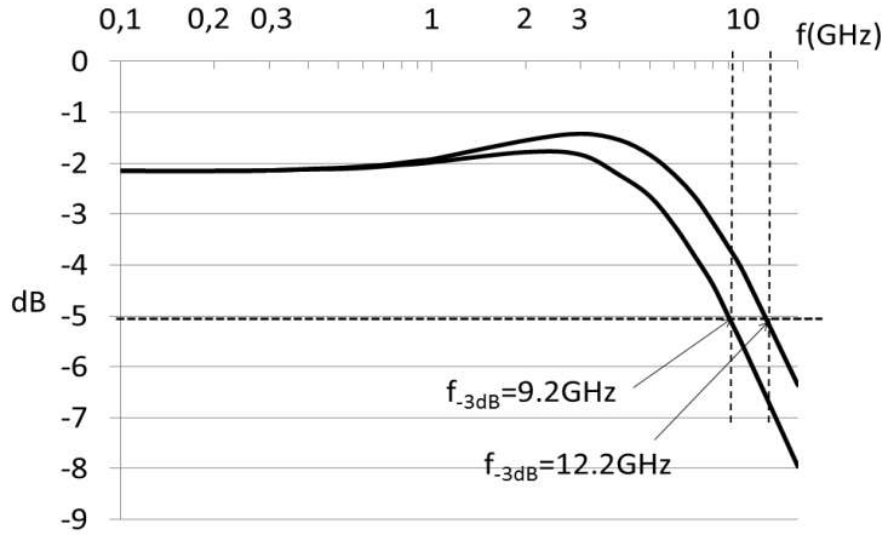
Fig. 12. Simulation of bandwidth extension technique (R_{WBE} as a parameter)
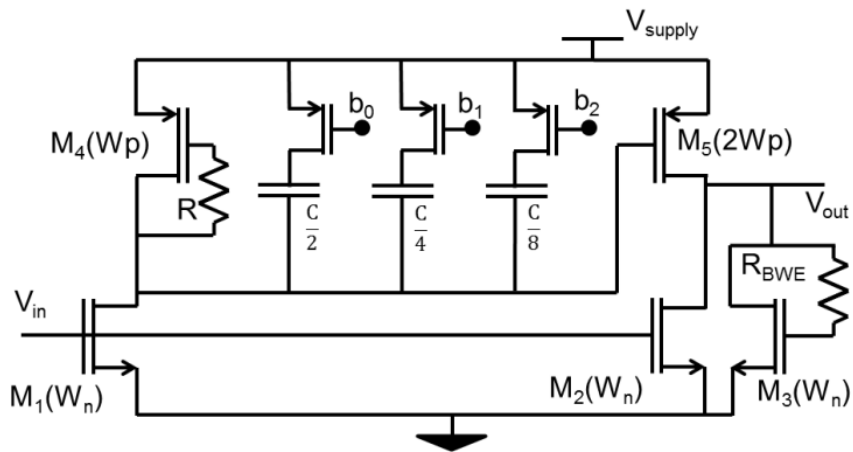
Fig. 13. The delay cell with 3 bit delay selection
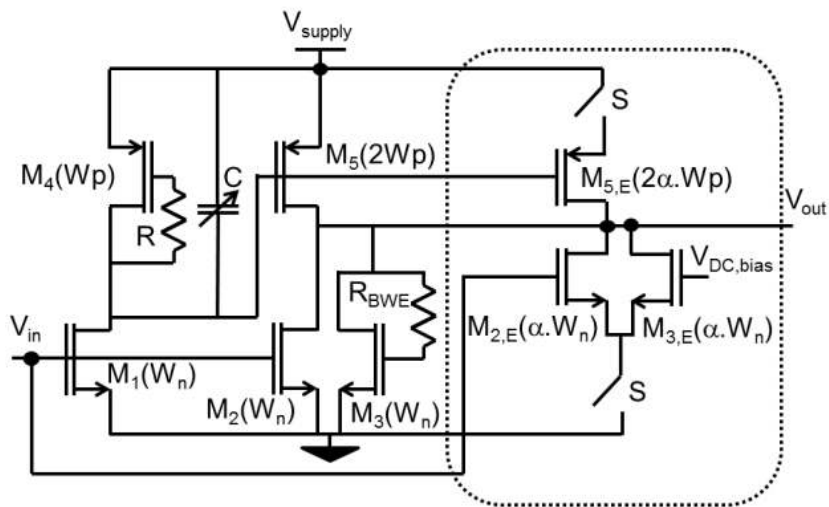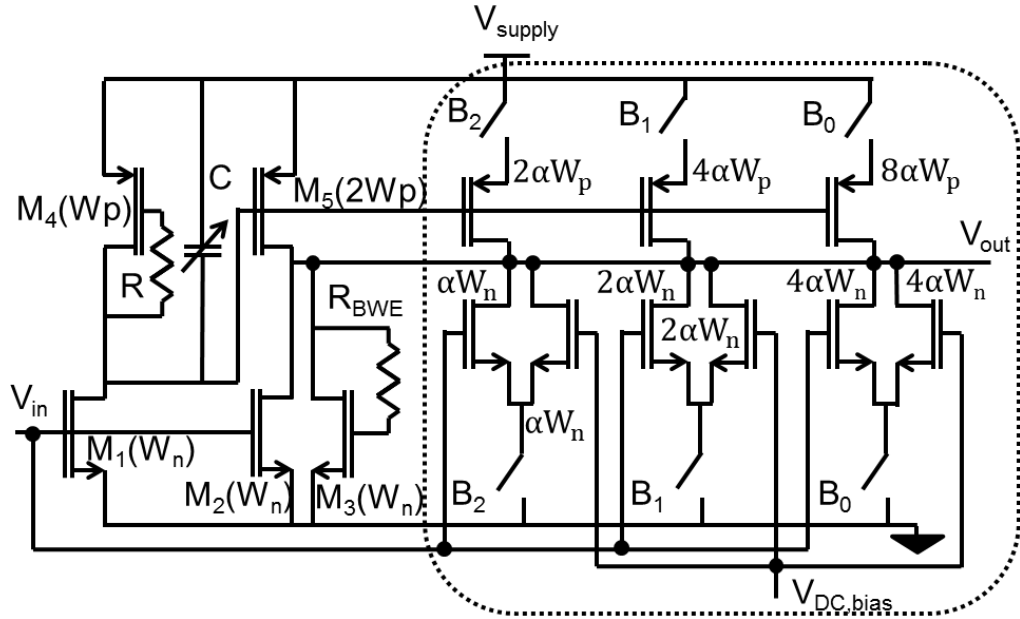

Fig. 14. Adding gain tuner to the delay cell

Fig.15. Adding 3-bit gain calibration to the filter

	Fig.3a [11]	Fig.3b [2]	This work
$V_{GS,nmos}$ (V)	0.714	0.714	0.714
$V_{GS,pmos}$ (V)	-	-	1.086
$V_{th,nmos}$(V)	0.427	0.427	0.427
$V_{th,pmos}$(V)	-	-	0.449
I_{DC} (mA)	0.2	3.4	0.6
Pole f_p (GHz)	0.36	0.48	2.63
Input referred noise @f_p (nV/sqrt(Hz))	12.8	2.4	6.2
IIP_3 (dBm@50Ω) @f_p	3	5	3
$V_{IM3=1\%}$ (mV)	48	84	45
SNR @ IM3=1% in BW=0.1GHz	52	71	57
Normalized SNR/P (1%IM$_3$,1Hz,1mW [20])	138	145	139

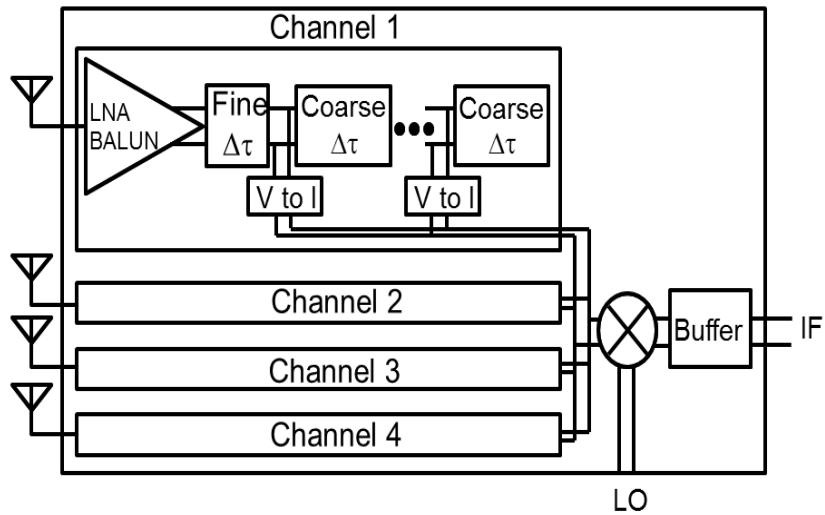Table 2. Comparison between simulated delay cells

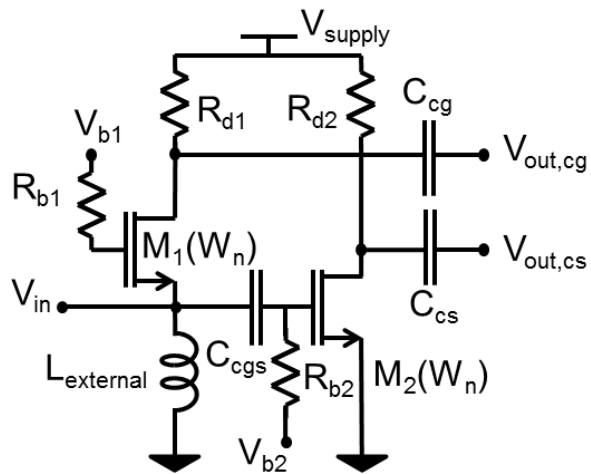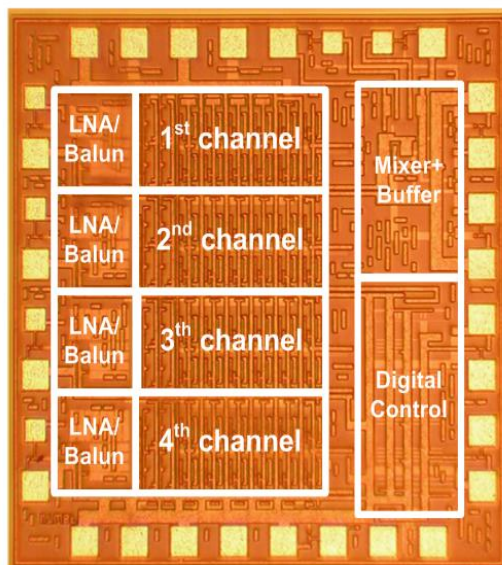Fig.16. The timed array IC: block level **[12]**
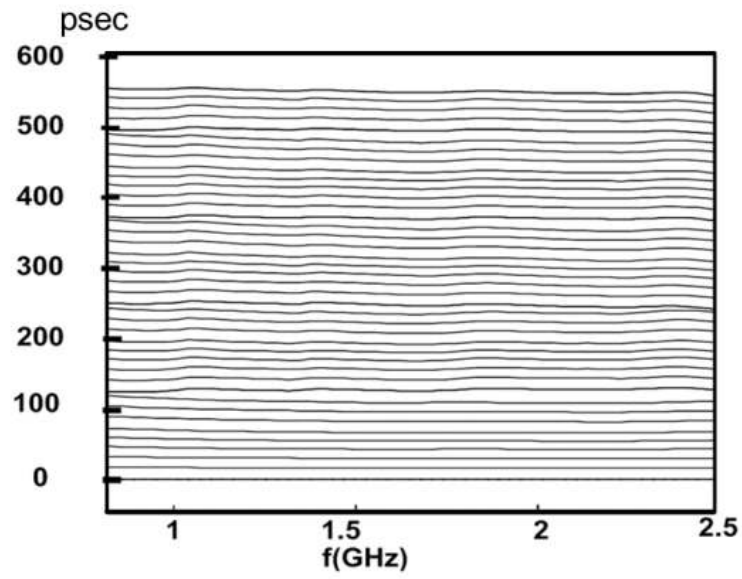

Fig. 17. LNA/BALUN

Fig. 18. The chip photograph

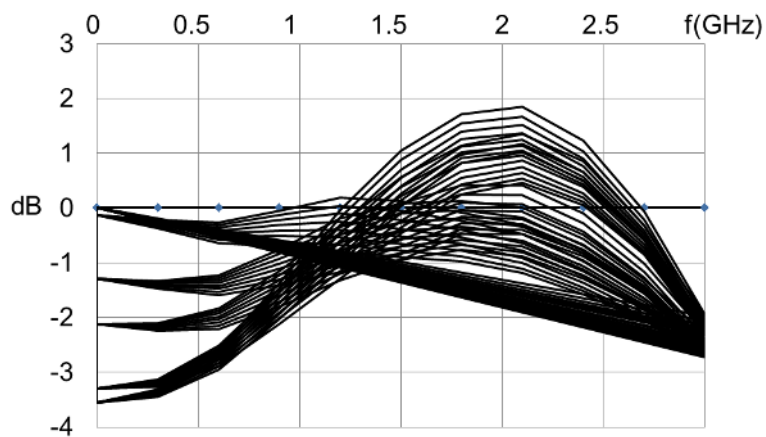Fig. 19. Delay versus frequency for all delay settings.

Fig.20. Gain of the delay line (fine tune and coarse tune) vs. f for all delay settings
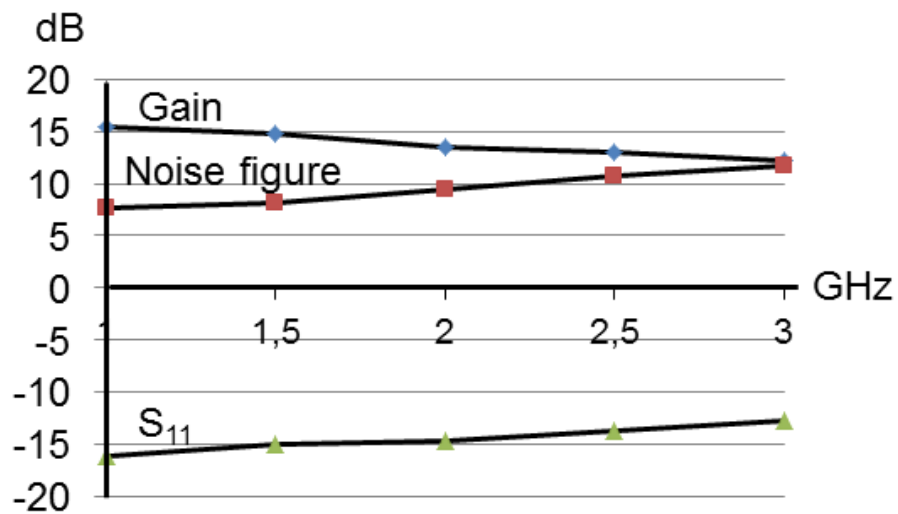

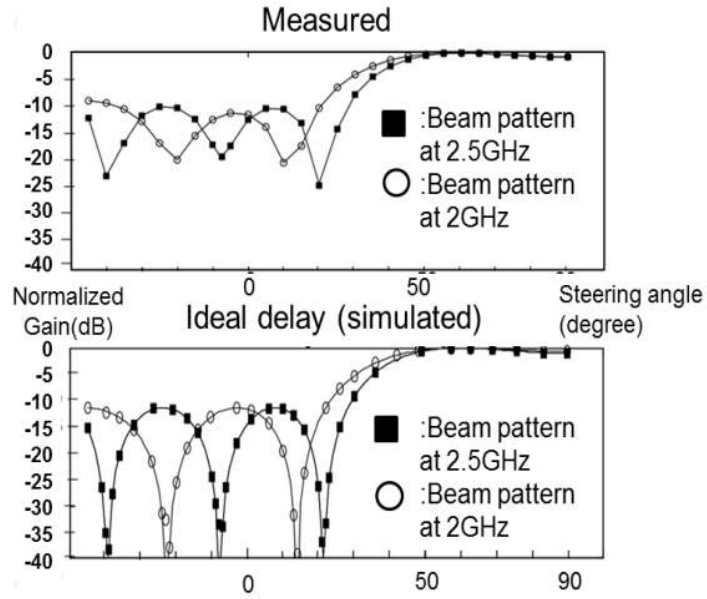Fig. 21. Gain, input matching and noise figure when delay of the channel is 255ps.

Fig. 22. The measure beam pattern compared to a simulated ideal beam pattern.

	[21]	[22]	[23]	[9]	[24]	[25]	[26]		[26]		This work
Technology	0.18 μm SiGe	0.13 μm SiGe	0.13 μm SiGe	0.13 μm CMOS	0.8 μm SiGe	0.09 μm CMOS	0.25 μm SiGe		0.25 μm SiGe		0.14 μm CMOS
Supply Voltage(V)	2.5	2.5	2.5	1.5	2.5	N/A	2.7		1.5		1.5
Gain variation(dB)	±1	N/A	N/A	±3	±0.7	±3	±0.9		±1.4		±1.4
Max. delay(ps)	64	16	54	225	25	26	12		12.5		550
Frequency[GHz]	1-15	55-65	31-41	1-15	3-10	0-8	20-40	25-35	20-40	25-35	1-2.5
Delay variation	~16 %	N/A	N/A	~14%	40%	10%	6.4 %	3%	6.6 %	3.2%	1.8%
P_{DC}/channel(mW)	87.5	-	104	78	38.5	-	146		33		90
Resolution(ps)	4	1.2	18	15	Cont.	13	Cont.		Cont.		13
Size(mm^2)	0.82	0.35	1.44	1.5	0.23	N/A	0.1		0.1		0.07
Delay/Size (ps/mm^2)	78	45	37.5	150	109	N/A	120		125		7857

Table 3. benchmarking and comparison between different reported delay cells.

	This work	Chu, ISSCC 2007 [9]	Van Vliet, GAAS 2003 [8]
Technology	CMOS, 140nm	CMOS, 130nm	PHEMT, 250nm
Technique	Gm-C	LC delay	Transmission line
Features Per Antenna Channel			
Gain	12-15dB (f-dependent)	10dB	6-9dB
Noise Figure	8-10dB	2.9-4.8dB	4.3dB
IIP3	-13 to -20dBm (min to max delay length)	Not mentioned	Not mentioned
-1dB compression point	-21 to -28 dBm (min to max delay length)	Not mentioned	5dBm
Amplitude variation vs. f	$\pm$1.4dB	$\pm$1dB	$\pm$2.5dB
Delay resolution	14psec	15psec	2.5psec
Delay variation vs. f	<10psec	<40psec	<20psec
Maximum delay	550psec	225psec	150psec
Current consumption	50mA	40mA	Not mentioned
Complete 4 channel beamformer			
Beam direction resolution	3.5Bit	3.5Bit	6Bit
Bandwidth	1-2.5GHz	18GHz	3-16GHz
Power consumption	250mA@1.8V	370mA@1.5V	Not mentioned
Die area	1mm^2	10mm^2	10mm^2

Table 4. Comparison between this works and two other time delay based timed array systems